ELSEVIER

Global and Planetary Change 9 (1994) 115–131

GLOBAL AND PLANETARY CHANGE

An energy balance model for the Greenland ice sheet

R.S.W. van de Wal, J. Oerlemans

Institute for Marine and Atmospheric Research, Utrecht University, Princetonplein 5, 3584 CC Utrecht, The Netherlands

(Received September 10, 1992; revised and accepted April 12, 1993)

Abstract

The sensitivity of the mass balance of the Greenland Ice Sheet is studied by means of an energy balance model. The model calculates the shortwave and longwave radiation and the turbulent fluxes on a grid with a grid point spacing of 20 km. Special attention is given to the parameterization of the albedo. The albedo is calculated as a function of snow depth, ablation, amount of meltwater at the surface and the type of surface. The response of the model to changing climatic input is nonlinear. As a result the ablation drifts to higher values when temporal variability of input is imposed.

Climate change experiments reveal a large sensitivity of the mean ablation to small changes in the temperature. A 1K rise in temperature leads to approximately 30% more ablation. Further experiments with this model suggest that the contribution of the Greenland ice sheet to past global sea level rise has been 35 ± 18 mm over the last 120 years. Applying the Bellaggio scenario as a forcing function results in a doubling of the ablation by 2100 AD. The corresponding contribution to global sea level rise is 6 cm over the period 1985–2100 AD.

1. Introduction

The background to this study is the growing interest in the effects of possible greenhouse warming on sea level. Besides thermal expansion of the ocean and shrinkage of the volume of small glaciers and ice caps, the two major ice sheets, Antarctica and Greenland, might also contribute to sea level rise. The response of an ice sheet to changes in the climate is complicated. The interaction between ice flow, ice temperature and isostatic adjustment of the underlying bedrock depends on the way in which the mass balance is formulated. Here we restrict ourselves to the century time-scale; this means that we consider the ice flow, ice temperature and bedrock to be in steady state. Changes in the volume are then entirely due to changes in the mass balance. This approach is justified by the long characteristic time-scale of ice flow, ice temperature and bedrock adjustment (e.g. Huybrechts et al., 1991).

In principle, mass balance measurements can be done in the field, but because of the enormous extent of the ice sheet, model studies are required to support these measurements. On the basis of mass balance measurements, Braithwaite and Olesen (1984, 1989) calculated the effect that a change in temperature would have on the mass balance for two specific sites at the southwestern margin of the Greenland Ice Sheet. They used a degree–day method in which the ablation is proportional to the sum of positive daily temperatures. Ambach and Kuhn (1989) used this approach to calculate the altitudinal shift of the

SSDI 0921-8181(94)E0067-9

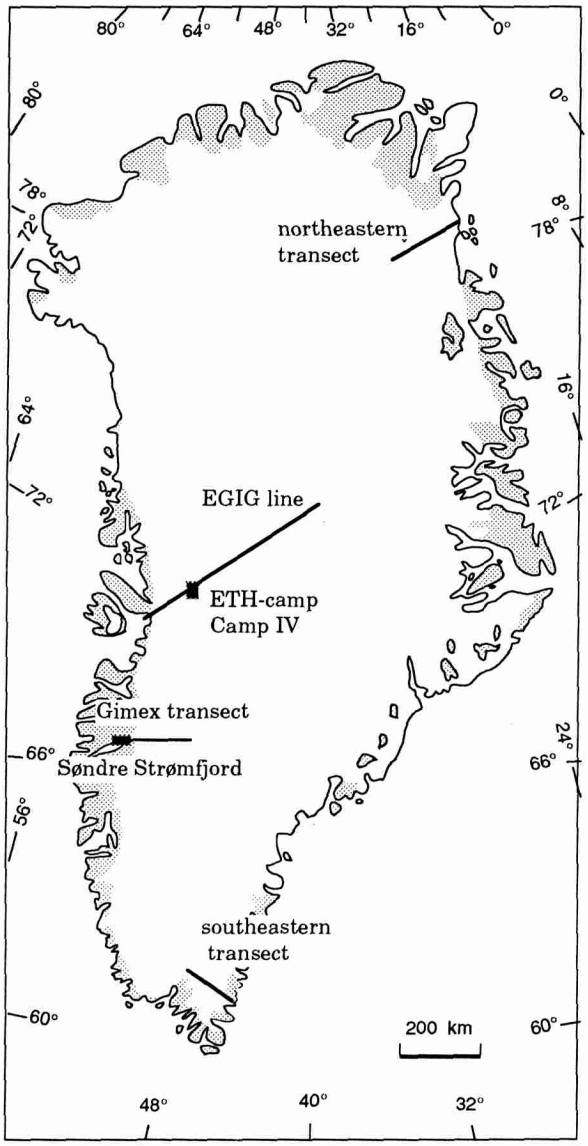

Fig. 1. Map of Greenland with topographical names used in this paper.

equilibrium line along the EGIG profile (Fig. 1). Reeh (1991) used the degree–day method to calculate the mass balance over the entire ice sheet.

The surface energy budget is treated more explicitly in energy balance models. Pioneering work on this method was done by Ambach (e.g. Ambach 1963, 1979). Braithwaite and Olesen (1990) applied the energy balance method to two glaciers in Southwest Greenland.

A more universal energy balance model for the entire ice sheet has been described by Oerlemans (1991). The present paper is an extension of this work. The main differences are the more detailed description of the albedo and a higher resolution in space and time. Some of the parameterization schemes are updated with recent field measurements from the GIMEx expeditions undertaken in the summers of 1990 and 1991 (Oerlemans and Vugts, 1993).

In the first section the model will be described. The model calculates shortwave and longwave radiation and the turbulent heat fluxes on a grid with a grid point distance of 20 km. The main input parameters are temperature, cloudiness, precipitation and the position of a grid point defined by the latitude, longitude and height above sea level. The most essential output parameter is the specific balance. The model has a time step of 40 minutes which allows a simulation of the daily cycle. Because the model is an extended version of a model presented by Oerlemans (1991), only the main features will be described in the main text. The actual parameterization schemes of the shortwave and longwave radiation and the turbulent flux are described in the Appendix.

Sensitivity experiments show the impossibility of diagnosing the current state of the mass balance with this type of model and indicate its large sensitivity to small changes in air temperature. Furthermore, it will be demonstrated that the mass balance itself is time-dependent due to the slow adjustment of the albedo. A larger ablation results in a lower albedo at the end of a model year, which increases the ablation the following year. An experiment for an enhanced greenhouse-climate scenario clearly demonstrates this point. Finally an attempt is made to calculate the contribution of the Greenland Ice Sheet to global sea level rise over the last 120 years.

2. The energy balance model

The ablation is calculated on an irregular grid with a minimum grid spacing of 20 km. Fig. 2 gives an impression of the distribution of the 800

Fig. 2. The grid used in this work. The points form the 20×20 km grid, the energy balance calculations are done at the crosses, and then interpolated to the grid.

grid points over the ice sheet. The ablation on the other points (in the 20 km grid) is linearly interpolated from the first group of points; this results in a regular grid with 20 km spacing (the same as used by Letréguilly et al., 1991). Altogether this gives 4219 ice-covered grid points, representing an area of 1.69×10^6 km^2. A fixed height (h_s) is assigned to all grid points. The surface topography used is shown in Fig. 3.

Details on the parameterizations briefly described below can be found in the Appendix.

2.1. Ablation

The model solves the following energy balance:

$$B = (1-\alpha)Q + L_i + L_o + H + LE \qquad (1)$$

where B is the energy available for melting, α the surface albedo, Q the shortwave radiation, L the longwave radiation (i = incoming, o = outgoing), H the sensible heat flux and LE the latent heat flux. From now on energy fluxes towards the surface are considered positive, fluxes directed away from the surface negative. Heat transport in the upper firn and ice layers is parameterized by considering refreezing in a schematic way. It is assumed that in late spring and early summer a layer of 2 m ice equivalent has to be heated from the annual mean temperature to the melting point. The following formulation proposed by Oerlemans (1991) is adopted:

$$R = Be^{T_{ice}}$$

$$A_{ice} = B - R = B(1 - e^{T_{ice}}) \quad (T_{ice} \leq 0) \qquad (2)$$

So the fraction of energy used to melt ice or snow (R) increases as the ice temperature rises during the season. As a consequence, the fraction used to heat the ice layer (A_{ice}) decreases and vanishes as soon as the ice temperature $T_{ice} = 0$. With this approach the amount of refreezing equals the amount measured by Ambach (1963) at Camp IV. In order to simulate the daily cycle properly, the net loss of energy from the surface during the night has to be compensated in the morning before melting starts. This is particularly important later in the season when the ablation decreases. In the following section the processes involved in the different terms in Eq. (1) will be described, starting with the shortwave radiation.

2.2. Shortwave radiation

The shortwave radiation is calculated as a function of the following variables: time, latitude, altitude and cloud cover. To simplify the calculation all grid points are considered to be flat

squares. This is a reasonable assumption for the Greenland Ice Sheet where slopes are generally smaller than 1°. The radiation at the top of the atmosphere can be calculated from the position of the sun (e.g. Walraven, 1978).

To obtain the incoming shortwave radiation at the surface, atmospheric transmission coefficients have to be defined. We distinguish a transmission coefficient for a clear sky due to scattering and absorption by air molecules, ozone and water vapour, and a transmission coefficient for clouds. A natural approach is to specify clear sky transmissivity as a function of altitude and zenith angle.

Besides the clear sky transmission we have to define the influence of clouds on the shortwave radiation at the surface. This poses a problem, since the distribution of clouds in space and time has not been measured extensively. Mean values at meteorological stations in the coastal zone show a monotonous decrease of 40% going from South Greenland to North Greenland. Furthermore, we assume a 33% reduction in the cloud cover from the ice margin to the central part of the ice sheet. This reduction in the central part is used in our calculation although only very few long-term measurements of cloud cover are available for this part of the ice sheet. The distribution of the cloud cover used is presented in Fig. 4.

2.3. Longwave radiation

The longwave radiation is parameterized using height above sea level and cloud cover, as previously described, and air temperature. For this purpose we used a compilation of temperature data presented by Ohmura (1987) (mean annual air temperature and seasonal cycle). Since we simulate the daily cycle we also define a daily amplitude. The calculation of incoming longwave radiation follows the method proposed by Kimball et al. (1982). The radiation has two components, one originating from the clear sky and one originating from clouds. The outgoing longwave radiation is determined by the surface temperature, which is a function of the air temperature.

2.4. Turbulent fluxes

The last two terms in Eq. (1), $(H + LE)$, the turbulent heat fluxes, are assumed to be proportional to the temperature difference between atmosphere and surface. A separate treatment of the latent heat flux has not been attempted. Field measurements along a profile near Søndre Strømfjord show a decreasing turbulent heat flux with height. Close to the margin a sensible heat flux directed towards the surface can be observed and a negligible latent heat flux (Van de Wal and Russell, 1994; Duynkerke and van den Broeke, 1994). Around the equilibrium line, the measurements done by the Free University (Vugts, pers. comm., 1992) indicate an equilibrium between the latent and sensible heat flux. These observations are reflected in the parameterization of the turbulent heat flux through an exchange coefficient that decreases rapidly with distance from the margin (x). The absolute magnitude of the exchange coefficient near the margin, 10 W m^{-2} K^{-1} is in the range usually found in the literature (e.g. Kuhn, 1979, 1989; Greuell and Oerlemans, 1989).

2.5. Accumulation

Although we do not explicitly calculate the accumulation with this model, some brief remarks are in order because accumulation plays an important role in the parameterization of the albedo. The annual accumulation is taken from Ohmura and Reeh (1991), who made a compilation from measurements in the period 1913–1989. Their map seems to be the best currently available. The distribution of accumulation through the year is based on the general impression obtained from coastal stations (Putnins, 1970). In the summer and autumn months (July–November) the accumulation is assumed to be twice as high as in the other months. Furthermore, accumulation occurs every third day.

In the section which describes the reference experiment, the result of the parameterization schemes for shortwave radiation, longwave radiation and turbulent heat flux along the Søndre

Strømfjord transect will be shown. The only remaining quantity needed to solve the energy balance now is the albedo.

3. The albedo parameterization

Since shortwave radiation is the major source of energy in the energy balance, the albedo parameterization plays an important role. With the following model an attempt is made to simulate the physical characteristics of the albedo of a glacierized area. The albedo immediately after a snowfall event is high ($\alpha_{sn} = 0.85$), but decreases as the snow settles ($\alpha_{so} = 0.65$). At the beginning of the ablation season, one can observe a rapid decrease in albedo due to the presence of meltwater in the snow pack or at the surface. This water drains slowly due to the permeability of the snow and the small surface slope or it refreezes again. Once the snow has melted and the meltwater removed, the surface consists of bare ice, for which a constant value of 0.55 (α_i) is adopted for the albedo. The different characteristic zones for the albedo can be seen on a satellite image for July 25, 1991 (Fig. 5). The figure shows a large dry snow zone with a high albedo ($\alpha = 0.8$–0.9), bordered by a zone with a low albedo, the wet snow zone ($\alpha = 0.3$–0.4) and a bare ice zone ($\alpha = 0.5$–0.6).

To quantify the albedo of the different areas we consider the measurements of the albedo made during the GIMEx expedition in 1991 as summarized in Fig. 6. Site 4 and site 5 are in the bare ice zone with constant albedo (0.55) over the entire period. At this time of the year, site 6 is in the transition zone, showing a decreasing albedo in the course of time. Site 9 is around the equilibrium line, where the albedo is determined mainly by the accumulation events which increase the

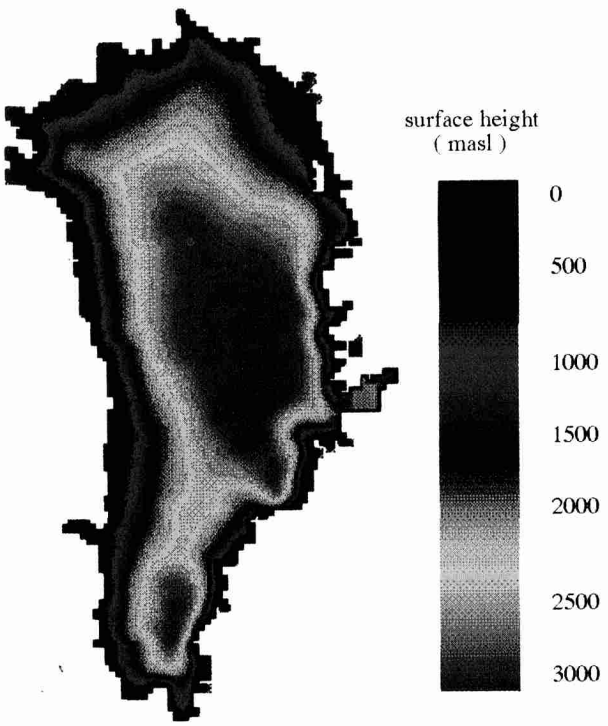

Fig. 3. The surface topography of the ice sheet.

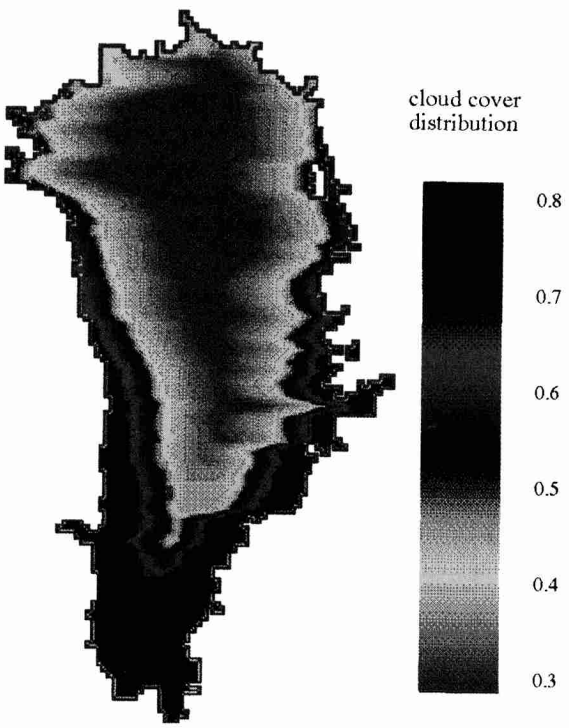

Fig. 4. The cloud cover distribution over the Greenland Ice Sheet, used as input for the energy balance model. Cloudiness is low in the central and nothern parts of the ice sheet, and high in the marginal zones in the southern parts.

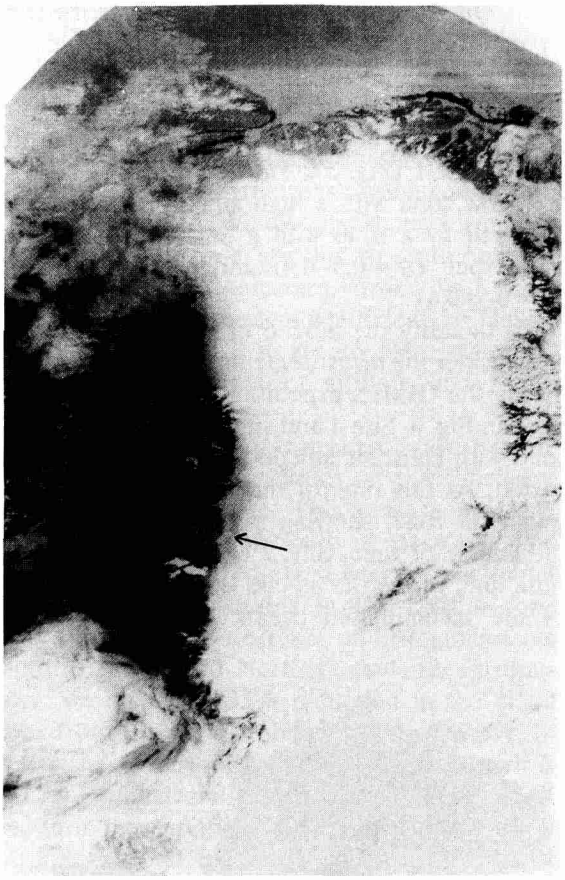

Fig. 5. NOAA-10 image of Greenland, taken on July 25, 12:04 UT (AVHRR, Channel 2). Note the dark band on the ice sheet in the study area (arrow), showing decreased albedo due to accumulation of melt water at the surface. Courtesy Danish Meteorological Institute.

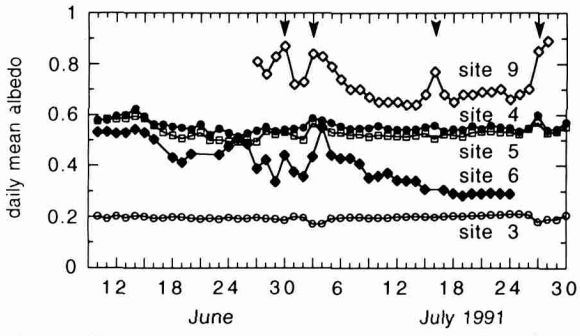

Fig. 6. Albedo measurements along the Søndre Strømfjord transect carried out during GIMEX-91. The data from site 9 are from the Free University. Site 4 and 5 are in the bare ice zone, site 6 is in the transition zone and site 9 in the accumulation zone. Precipitation events are marked with arrows.

albedo. After snowfall events, the albedo drops again in time.

The parameterization adopted to model these processes is presented schematically in figure 7. The albedo is calculated once a day, starting on January 1; the fraction of the surface covered with water (w) is assumed to be 0. Accumulation increases snow depth (d). The time after a snowfall event (τ) is then set to zero again. The water fraction changes via the integrated ablation over a day. The factor $-2/13$ represents the runoff rate of the water. Using this parameterization the water drains in approximately 13 days. This arbitrarily chosen parameter guarantees a rapid tran-

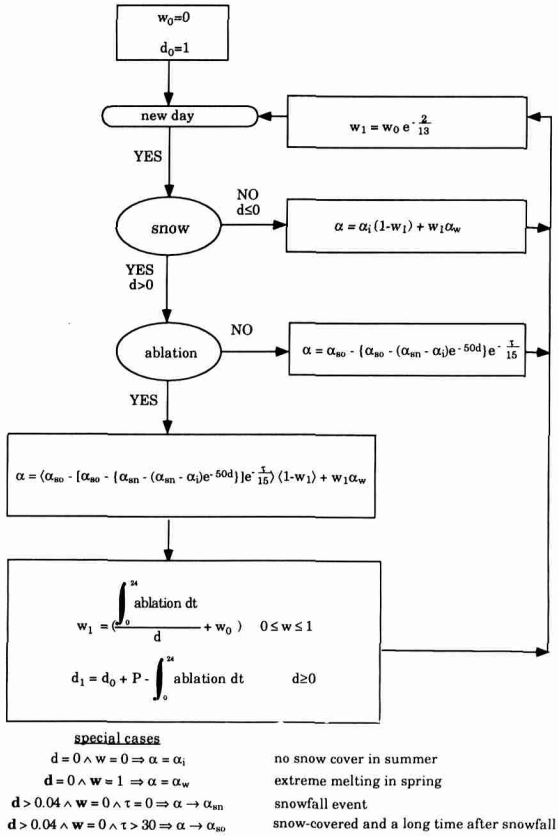

Fig. 7. The scheme for the calculation of the albedo [d is snow depth, t time after a snowfall event, w fraction of the surface covered with water, $\alpha_i = 0.55$ (albedo of bare ice), $\alpha_w = 0.2$ (albedo of water-covered ice, $\alpha_{sn} = 0.85$ (albedo fresh snow), $\alpha_{so} = 0.65$ (albedo of old snow)]. The subscript '1' refers to the day for which the albedo is calculated and the subscript '0' to the previous day.

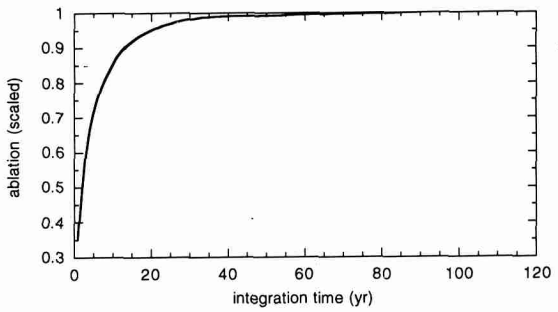

Fig. 8. The increase in ablation (averaged over entire ice sheet) towards a steady state value, starting from a uniform one-metre snow cover. The response time appears to be about 10 years.

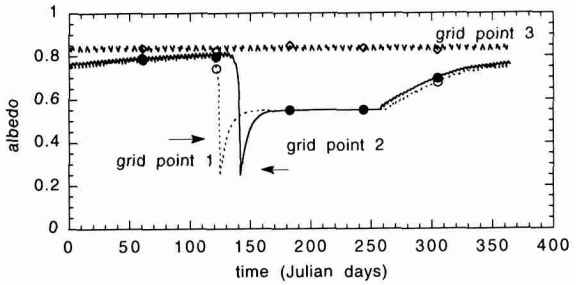

Fig. 9. The calculated albedo as a function of time for three different grid points along a transect near Søndre Strømfjord. The grid points 1, 2 and 3 are at a height of 265, 667 and 1603 masl, respectively.

sition from the winter snow cover to the summer bare ice period, as observed near the western margin. Altogether these processes specify the change in the albedo at all sites during the year. The lower most block in Fig. 7 shows how the snow depth and water content change by ablation and accumulation. At the bottom of Fig. 7 some special cases are presented to clarify the albedo parameterization.

The albedo for a grid point depends on the local balance of accumulation and ablation. The model integration starts with a snow depth of one metre over the entire domain. It then takes quite some years to obtain an equilibrium snow depth distribution. The response time of the system, defined as the time it takes to reach $(1 - 1/e^2)$ of the equilibrium value, is typically 10 yr. In Fig. 8 the ablation, scaled by the equilibrium state ablation, is plotted as a function of time to illustrate the response time of the system to one metre of snow cover over the entire ice sheet.

The result of the parameterization of the albedo is illustrated in Fig. 9 for a cross-profile near Søndre Strømfjord. At the beginning of the ablation season the albedo drops rapidly at sites 1 and 2, due to the presence of meltwater at the surface. As illustrated in the figure, the drop in the albedo occurs later in the season for site 2, which is higher up on the ice sheet. After some time typically one month, water and snow have melted and drained, and the albedo equals the albedo of ice which is 0.55. At the end of the season the albedo increases very slowly due to the small accumulation in this area. The high frequency noise at site 3 in the accumulation zone is

Table 1
A comparison between measured meteorological variables and energy fluxes, and modelled values for two sites. Note that the grid points do not match the locations in the field exactly. The measurements in Søndre Strømfjord were carried out in 1990 and those at the ETH camp in 1990. Data from ETH are presented by Greuell (1992). Q is shortwave radiation, α albedo, L_n net longwave radiation and F_l the turbulent flux.

	SFJ 1991		ETH 1990	
	measured	model	measured	model
Period	June 10–July 31	June 10–July 31	June 1–August 31	June 1–August 31
Latitude (°N)	67.05	66.9	69.34	69.8
Height (m.a.s.l.)	340	265	1155	1106
Cloud cover (%)	0.46	0.67	0.52	0.60
Air temperature (°C)	4.7	7.3	−0.7	+0.7
$Q(1-\alpha)$ (W m^{-2})	117	84	86	73
L_n (W m^{-2})	2	−16	−61	−43
F_l (W m^{-2})	43	69	9	14

caused by the snow that falls every third day. The albedo in the accumulation zone is therefore effectively slightly lower than the albedo of fresh snow.

4. The reference experiment

To test the sensitivity of the specific balance to climatic change we first define a reference state. This was obtained by running the model to a stationary state (using model formulation as given in the Appendix). In Figs. 10–14 and Table 1 the reference state is diagnosed.

Fig. 10 shows the specific balance. Large negative values are found in the ablation zone along the margin. Positive values decrease towards the north as a result of decreasing accumulation. Integrated over the entire ice sheet the ablation is 0.189 m w.e. or 54% of the mean annual accumulation. Fig. 10 illustrates that 88% of the modelled ice sheet is accumulation area and 12% ablation area, which is in agreement with the estimates of 90% for the accumulation zone and 10% for the ablation zone as presented by Reeh (1989). The large ablation areas are on the western side of the ice sheet. Due to the difference in area of accumulation and ablation zones, the mean ablation has to be approximately five times the mean accumulation (assuming ablation and calving to be equal) to obtain equilibrium between the mass gain and loss over a year.

Fig. 11 shows the distribution absorbed shortwave radiation in terms of annual mean values. The distribution is strongly influenced by the albedo, of course. Along the margin the absorbed shortwave radiation reaches a maximum due to the relatively low albedo. Further inland the absorbed shortwave radiation increases again, because of decreasing atmospheric transmissivity

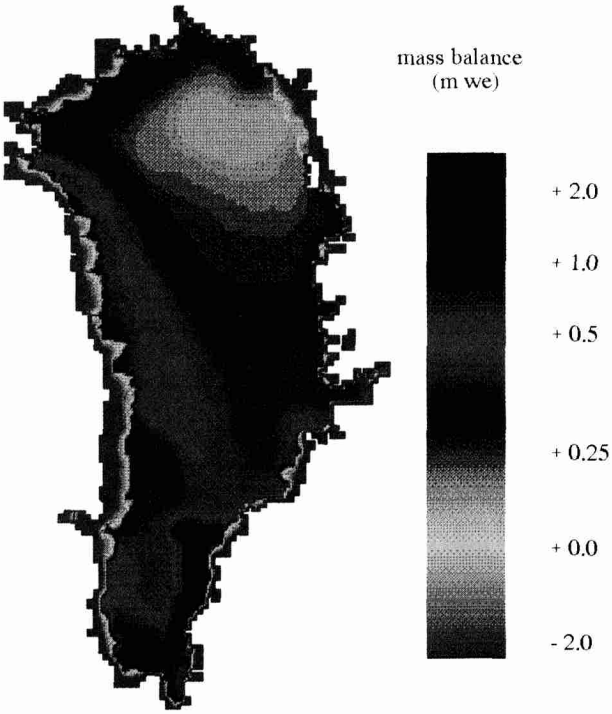

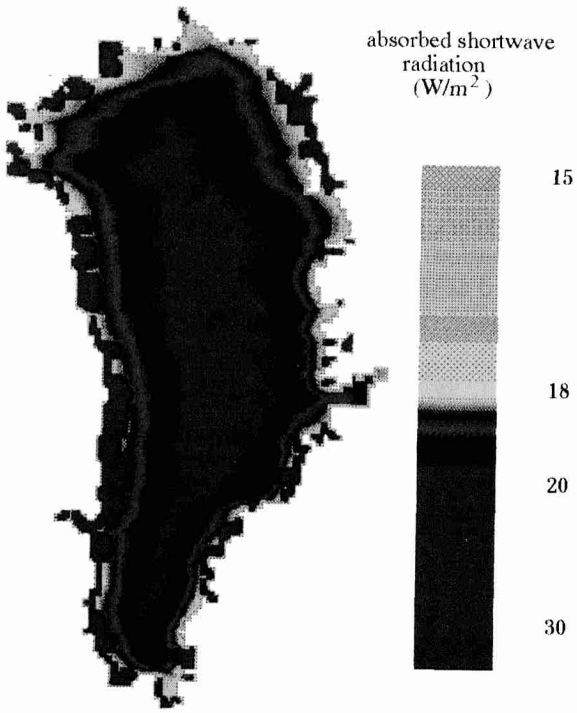

Fig. 10. The calculated mass balance distribution over the entire ice sheet. Note the non-linear scale. The output data have been filtered (3*3).

Fig. 11. The absorbed shortwave radiation calculated by the model. Note the minimum in the vicinity of the equilibrum line.

(mainly due to decreasing cloud cover). So there is a zone of minimum absorption in the vicinity of the equilibrium line. The ratio between the maximum absorbed shortwave radiation and the minimum is about 2.

When comparing the energy fluxes over the entire ice sheet, we found that 40% of the energy needed for the ablation (0.189 m w.e. = 100%) originates from the turbulent heat flux and 60% from the radiation balance. The contribution of the turbulent heat flux even increases to 50–60% in the southern and southeastern parts, whereas the contribution of the radiation balance increases to 85% in the cold and sunny northeastern parts. If we split up the radiation balance in the shortwave and the longwave component, it appears that the contribution of the shortwave radiation is +200% and the contribution of the longwave radiation is −140% (net radiation balance +60%). This means that, averaged over the entire ice sheet during the ablation period, the absorbed shortwave radiation is roughly 5 times as large as the turbulent heat flux. Nevertheless the radiation balance contributes only 60% of the energy needed for the ablation (integrated over the entire ice sheet) because the longwave radiation largely compensates for the shortwave radiation.

A more detailed picture of the different energy sources is presented in a cross-profile near Søndre Strømfjord, see Fig. 12. The absorbed shortwave radiation reaches a minimum around the equilibrium line at 1500 m.a.s.l., and then slowly increases again with increasing height. The turbulent heat flux decreases rapidly going from the margin towards the interior, as observed in the field, and the reduction of the longwave radiation is simply due to the lower air temperature at higher elevations.

In Table 1, a comparison is presented between results obtained with the model and recent meteorological observations. It is questionable whether it is useful to compare measurements on a timescale of one month with model results based on 10 year mean values. Nevertheless, we think it provides at least an idea of the importance of the various terms in the energy balance. For the ETH camp the slightly lower absorbed shortwave radiation calculated by the model can be explained by the higher cloud cover. Also, a slightly higher temperature contributes to the higher net longwave radiation. For the Søndre Strømfjord area the differences between the model and the measurements are larger, probably due to the very sunny weather during the measurements and the lower altitude of the model grid point, both resulting in an very high temperature. Because of these differences the ratio between the contribution of the turbulent flux and the shortwave radiation differs significantly. In the model 45% of the energy available for melting originates from the turbulent flux, whereas according to the measurements only 25% originates from the turbulent flux. The difference in the measured longwave radiation and the model values cannot be explained by differences in cloud cover and temperature since higher cloud cover and higher temperature result in a higher net longwave radiation as can be seen from Table 1. The best way of comparing the model with the field measurements is probably to compare calculated and observed mass balance gradients. Unfortunately not many mass balance measurements are available yet. Large gradients in the mass balance can be observed in the warm and wet southeastern sector and low mass balance gradients in the cold and dry northeastern sector. The reference experiment yields a mass balance profile near Søndre Strømfjord which can be compared with the abla-

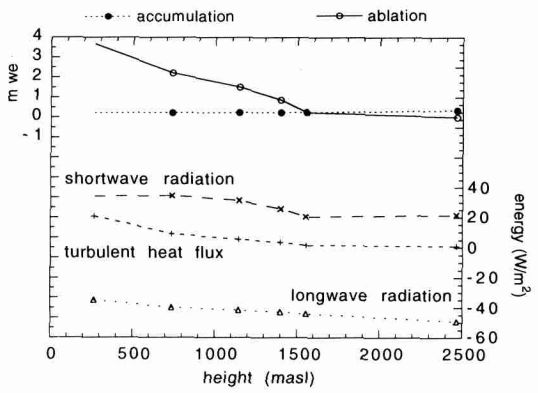

Fig. 12. Accumulation, ablation, and components of the mass balance (horizontal left axis) as a function of height for a transect near Søndre Strømfjord.

tion measurements (Van de Wal and Russell, 1994). A reasonable agreement between measured and modelled profiles can be seen in Fig. 13c. In Fig. 13a, d a similar comparison between measured and modelled ablation profiles is presented for different regions. In general reasonable results are obtained with the model, but one peculiarity should be noted. The model calculates too high an equilibrium line altitude at the EGIG profile. An explanation for the observed differences in the mass balance gradient can be a result of the presence of a tundra in the Søndre Strømfjord area where there is almost no tundra close to the EGIG line. Due to the presence of a tundra warm air is transported from the tundra towards the ablation area, increasing the turbulent heat flux (Van den Broeke et al., 1994). This process may well lead to steeper mass balance gradients. Because the model does not incorporate this effect, differences in the measured and modelled mass balance gradient might be expected between the EGIG line and the Søndre Strømfjord area. Nevertheless the large mass balance gradients on the southeastern side of 5–6 mm w.e. m^{-1} yr^{-1} and 2–4 mm w.e. m^{-1} yr^{-1} in the dry western and northern areas are in good agreement with measurements (Humlum, pers. comm., 1991; Weidick, 1984).

5. Sensitivity experiments

Changing one parameter in the model and keeping all others fixed gives insight into the sensitivity of the model to the perturbed parameter. In Fig. 14 changes in the mass balance are

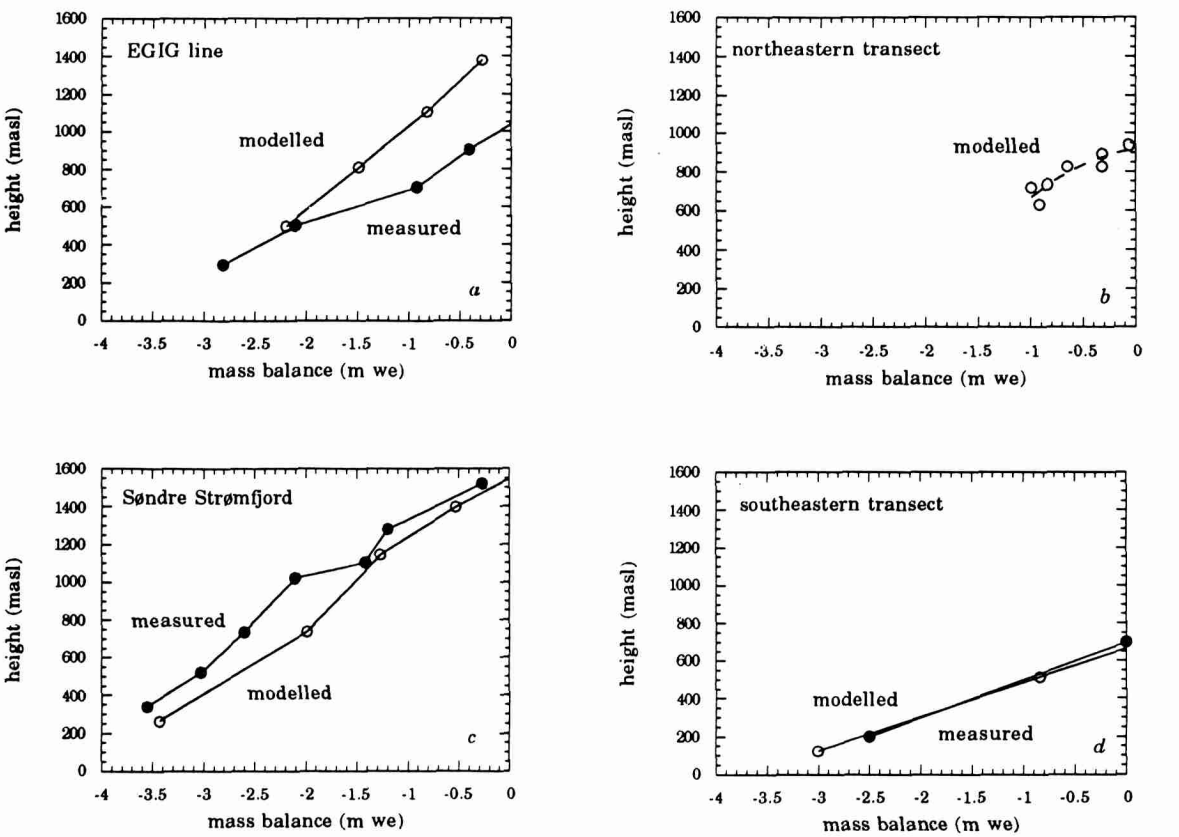

Fig. 13. Measured and modelled ablation as a function of height for four profiles. The points in figure 13b are a composition of points in this sector rather than a transect perpendicular to the ice margin.

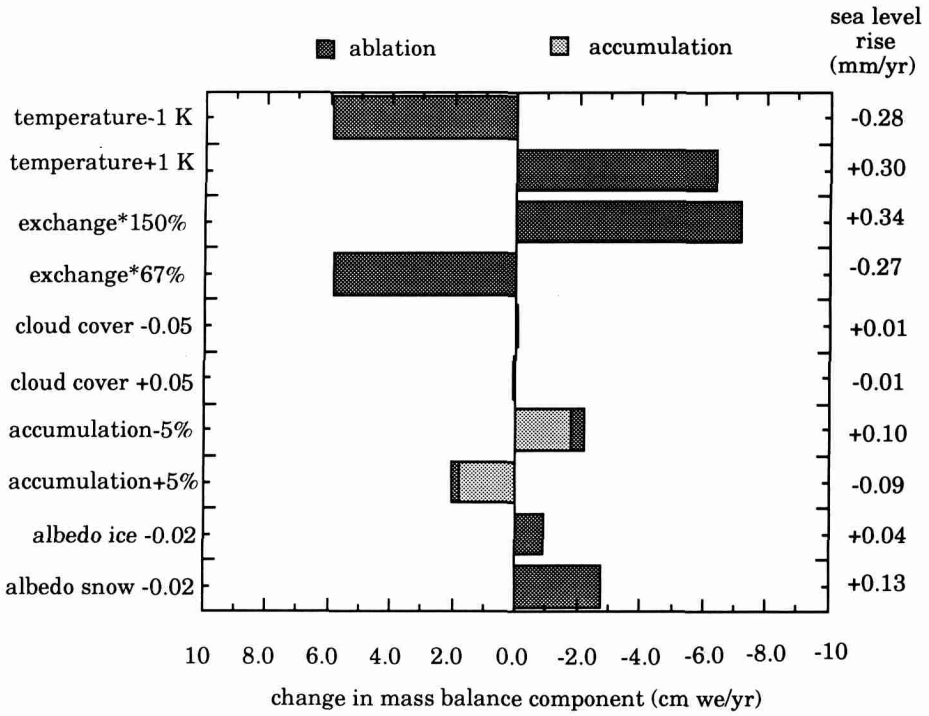

Fig. 14. The sensitivity of the model to changes in input parameters. On the right side of the figure the corresponding global mean sea level change is listed. The sensitivity is expressed as a change in the balance component (accumulation and ablation) in cmwe. A positive change (to the left!) means an increase in accumulation or a decrease in ablation. Note that the mean ablation for the reference experiment is 18.9 cmwe.

presented as a function of a change in a model parameter. The most outstanding are the sensitivity to a 1K temperature change and the sensitivity to the formulation of the exchange coefficient used to calculate the turbulent flux. This means that the uncertainty in the temperature field of approximately 1K, and the uncertainty in the formulation of the turbulent flux do not allow us to make any reliable estimates of the present state of balance with this type of model. Nevertheless, the sensitivity to a temperature change indicates the large sensitivity of the mass balance to a realistic climate change. The temperature sensitivity calculated with this model is at the lower end of earlier estimates of the temperature sensitivity listed by Warrick and Oerlemans (1990), varying from 0.31 to 0.48 mm global mean sea level rise per degree C.

Fig. 14 also shows that changes in the cloud cover do not significantly alter the mass balance of the entire ice sheet. Increased cloud cover not only reduces the shortwave radiation, but also increases the longwave radiation, resulting in a net negligible effect integrated over the entire ice sheet. However, this result should be considered too preliminary as long as the applied parameterization for the cloud cover is based on measurements in the Alps. It should be possible to study the dependence of the mass balance on cloud cover in the near future once a parameterization based on measurements in Greenland is incorporated in the energy balance model (Konzelmann et al., 1994).

Fig. 14 also reveals an asymmetry of the response to a negative or a positive perturbation. The increase in ablation caused by a rise in

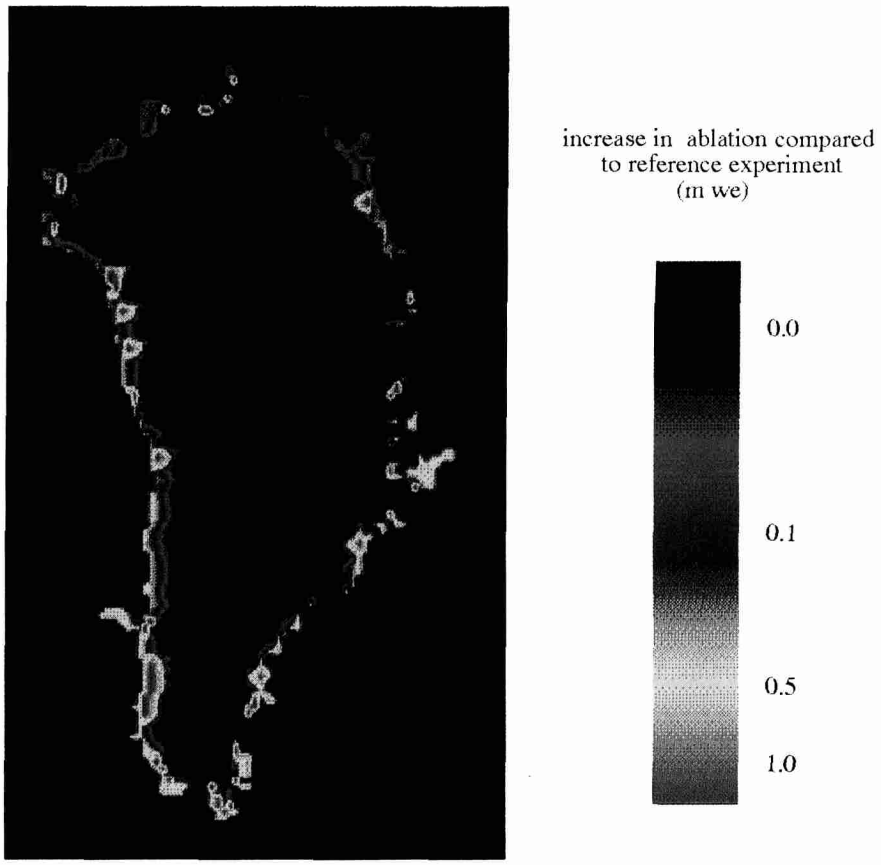

Fig. 15. The increase in the ablation as a result of a 1K temperature increase.

temperature is larger than the decrease in ablation caused by an equivalent drop in temperature. This means that a random distribution of temperature or any climate variable, around the present state would slowly increase the ablation.

6. Climate-change experiments

In Fig. 15 the distribution of the increased ablation for a 1K temperature rise is presented for the entire ice sheet. Obviously not much will change in the centre of the ice sheet but the increased ablation along the margin will cause a net increase of 0.063 m w.e. in the mean ablation. The largest changes are observed in the south-western part of the ice sheet. Fig. 16 shows the changes in the ablation in more detail for a cross-profile near Søndre Strømfjord. The higher temperature leads to larger turbulent fluxes and therefore especially to greater ablation at low altitudes. The balance gradient thus steepens.

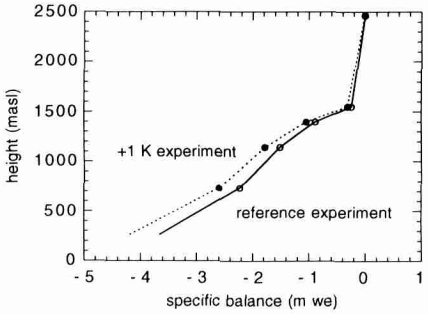

Fig. 16. The increase in the ablation for a transect near Søndre Strømfjord for a 1K temperature rise.

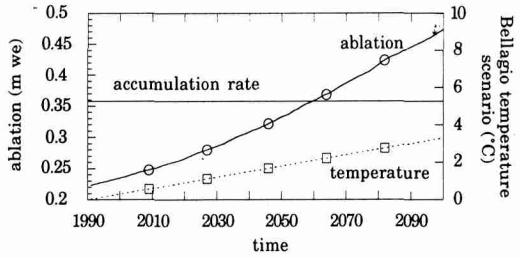

Fig. 17. The increase in the mean ablation in time when the Bellaggio temperature scenario is imposed.

Fig. 17 presents results for an enhanced greenhouse warming scenario. A uniform temperature perturbation, being a function of time, is imposed on the model. We used the "Bellaggio scenario" implying a nearly linear temperature rise of 0.3°C per decade. Since the different areas, like the dry northern area, and the wet southern area, might respond differently to a changing climate, predicting a change in the mean accumulation is necessarily very speculative. The order of magnitude of a change in accumulation is certainly smaller than a change in the ablation, so the accumulation is kept constant during the greenhouse experiment. The temperature forcing results in an increase of the ablation which will equal the accumulation in approximately 2060 AD. The mean ablation increases nonlinearly while temperature increases linearly. The model predicts a doubling of the ablation in 2100 AD, which corresponds to a global mean sea level rise of 56 mm over the period of integration.

On a longer time-scale the interaction between the mass balance, ice temperature and ice dynamics might reach a new equilibrium in a warmer climate. It is stressed that in this study only changes on a century time-scale are studied for a fixed geometry of the ice sheet.

A final experiment consists of a historical simulation of the mass balance of the Greenland Ice Sheet over the period 1870–1990. Such an experiment may give some insight into the contribution of the Greenland Ice Sheet to sea level rise in the recent past. To perform an experiment of this kind, one needs a historical record of all climate parameters used in the model. A lack of data limits the possibilities to a temperature and precipitation record as input. We used a compilation of annual mean temperature measurements at Greenland stations (provided by P.D. Jones). Annual mean values are used because the parameterized temperature field in the reference experiment refers to the annual mean temperature over the period 1951–1960 (Ohmura, 1987), see Fig. 18a. This is not necessarily the best because most ablation occurs in summer, but it introduces the most straightforward coupling with the reference experiment. A precipitation record was obtained from ice core analysis (Dibb et al., 1990), as presented in Fig. 18b. Note that the mean precipitation is constant over the entire period. Of course, one can argue whether the precipitation

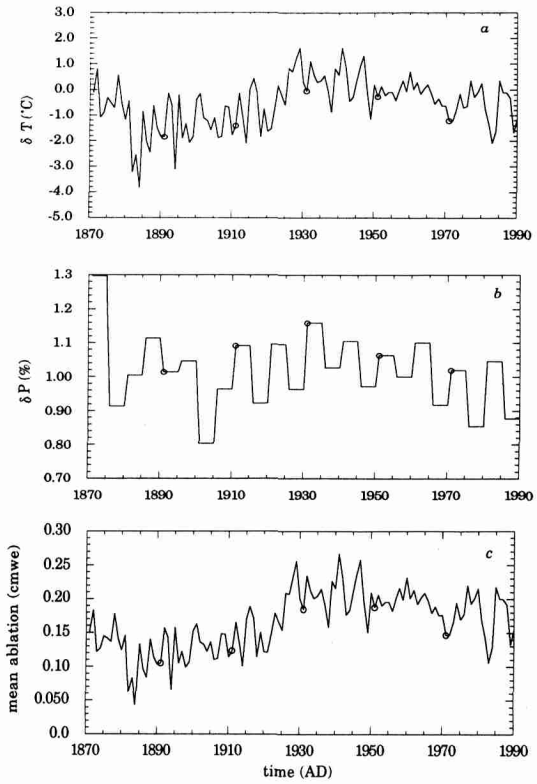

Fig. 18. Historical simulation of the mass balance of the Greenland Ice Sheet over the last century. The temperature record is presented as departures from the reference period 1951–1960 AD. The precipitation record is presented as departure from the entire period.

record of Summit is valid for the entire ice sheet, but at least no long term deviations between Summit and Dye 3 are observed (Dibb et al., 1990). The crucial point of this experiment is the definition of the initial state. Here a steady state is calculated for a temperature that is −1.17 K lower than in the reference experiment discussed earlier. This is the temperature difference between the periods 1871–1890 and 1951–1960 AD. The time integration then continues with the observed annual mean temperature and a precipitation record derived from ice core analysis. The result of the simulation is shown in Fig. 18c. A mean increase in the ablation of 53 mm w.e. over the period 1890–1990 can be calculated. This corresponds to a 25 mm contribution to sea level rise over the period 1890–1990 AD. It should be stressed, however, that this result is sensitive to the choice of the initial state.

The estimate obtained here is in agreement with the earlier estimate presented by Warrick and Oerlemans (1990), using (summer) temperature forcing with a fixed sensitivity of the mass balance of 0.3 ± 0.2 mm yr^{-1} per degree K.

7. Conclusions

The ablation on the Greenland ice sheet appears to be quite sensitivie to temperature change: a 1K temperature rise produces a 34% increase in the mean ablation, which is in agreement with earlier estimates using an energy balance model (Oerlemans, 1991). As the error in input temperature will be at least 1K, this also implies that it is impossible to diagnose the present state of balance by means of energy balance modelling (the same argument holds for the degree-day method, e.g. Reeh, 1991.

The energy balance model presented here is capable of reproducing realistic albedo patterns in space and time, at least qualitatively. However, a rigorous test of the albedo scheme can only be done when maps of surface albedo derived from satellite observations become available.

The results of energy balance models are most sensitive to the parameterization of the turbulent heat flux. Reducing the uncertainty in the parameterization of the turbulent heat flux by field measurements will improve these results. More generally, analyses of the existing data sets of the ETH at the EGIG line, the Free University and the University of Utrecht, will permit the parameterisations used in this model to be improved. The radiation schemes proposed in Konzelmann et al. (1994) should preferably be used for future energy balance models of the Greenland Ice Sheet.

The mass balance itself is a physical system with a response time and memory effects and not simply the summation of ablation and accumulation over a single year.

A warmer climate leads to steeper mass balance gradients due to the increase in the turbulent heat flux near the margin.

The Bellaggio scenario results in a doubling of the ablation, which corresponds to a global mean sea level rise of 56 ± 28 mm in 2100 AD.

The contribution of the Greenland Ice Sheet to the rise in the global mean sea level is estimated to have been 25 ± 13 mm over the last 100 years.

8. Acknowledgements

We are very grateful to Philippe Huybrechts for providing us with some data files for the Greenland Ice Sheet. We appreciate the interesting discussions we had with Michiel van den Broeke and thank him for his comments. We are indebted to Dr. P.D. Jones, University of East Anglia, for supplying the temperature data used in the historical simulation of the mass balance. Sheila McNab has helped with the English text.

This work was sponsored by the Netherlands Organisation for Scientific Research (Werkgemeenschap CO_2-Problematiek). Additional support was obtained from the Climate Programme of the European Commission, under contracts no. EVUC-0053-NL (GDF) and EPOC-CT90-0015, and from the Dutch National Research Programme on Global Air Pollution and Climate Change (contract 276/91-NOP).

9. Appendix—description of the parameterizations

In this section the three main components (shortwave, longwave, and turbulent flux) of the energy balance equation (1) are described. The symbols used in the equations are listed separately after the description of the turbulent heat flux.

Shortwave radiation

The shortwave radiation at the surface is calculated from the shortwave radiation at the top of the atmosphere according to:

$$Q = S\tau_a\tau_c \tag{3}$$

We distinguish a transmission coefficient for a clear sky and a transmission coefficient for clouds. The value of τ_a depends on altitude and zenith angle and can be parameterized by:

$$\tau_a = \left\{0.75 + 6.8\ 10^{-5}h_s - 7.1\ 10^{-9}(h_s)^2\right\} \times \{1 - 9\ 10^{-4}Z\} \tag{4}$$

The clear sky transmissivity is a schematic fit, based upon measurements during clear sky conditions in the summer of 1991. Three masts are used along a profile near the ice margin in Søndre Strømfjord. It should be noted, however, that the gradient of the radiation with height is considerably larger than the gradient calculated with a multi-level spectral shortwave radiation model. For details on this subject we refer to Konzelmann et al. (1994); here we simply used the measurements we obtained. Besides the transmission for clear skies we have to define the absorption of shortwave radiation by clouds as defined by:

$$\tau_c = 1 - \left(0.41 - 6.5\ 10^{-5}h_s\right)n - 0.37n^2 \tag{5}$$

The cloud cover parameterization is a fit resulting from measurements at glaciers in the Alps (Sauberer, 1955). An estimated cloud cover distribution is applied in the model according to:

$$n = \left(\frac{29.4}{\varphi - 23.3}\right)\left(\frac{1000 - x}{1000}\right) \tag{6}$$

This parameterization is based on the 10 and 20 year mean values for coastal meteorological stations indicating a decrease of 40% going from South to North Greenland (Putnins, 1970). In addition to this a 33% reduction in the cloud cover from the ice margin to the central parts is assumed.

Longwave radiation

The longwave radiation is parameterized using height above sea level, cloud cover and air temperature. Based on a compilation of temperature data by Ohmura (1987) the following parameterization for the annual mean temperature and the amplitude of the yearly cycle has been derived by Huybrechts et al. (1991):

$$\bar{T}_a = 49.13 - 7.992\ 10^{-3}h_s - 0.7576\varphi \quad h_s > h_{inv}$$

$$h_{inv} = 300\frac{\varphi - 65}{15}$$

$$\bar{T}_a = 49.13 - 7.992\ 10^{-3}h_{inv} - 0.7576\varphi \quad h_s \le h_{inv} \tag{7}$$

$$A_t = -18.35 + 0.00172h_s + 0.4314\varphi \tag{8}$$

A daily amplitude of the air temperature was defined to calculate the temperature during a day:

$$B_t = 4.0 + 0.0275x \tag{9}$$

The parameterization of the daily amplitude is in agreement with measurements near the ice margin (Van den Broeke et al., 1994) but is based mainly on data from Putnins (1970), which showed a daily cycle of 15°C in the central parts of the ice sheet during the summer months. Although the daily amplitude is known to change over the year, it is assumed for simplicity that the amplitude is independent of time.

To calculate the air temperature at a certain time step we assume a cosine function for the yearly cycle with a maximum at day 185 and a negative cosine function for the daily cycle with a maximum at solar noon as presented by:

$$T_a = \bar{T}_a - A_t\cos\left(\frac{2\pi(day - 3)}{365}\right) - B_t\cos\left(\frac{2\pi t}{24}\right) \tag{10}$$

The calculation of incoming longwave radiation on the basis of air temperature follows the method proposed by Kimball et al. (1982), where the radiation has two components, one originating from the clear sky and one originating from the cloud cover, Eqs. 11–15:

$$L_i = \epsilon_a \sigma T_a^4 + L_c \quad (11)$$

$$\epsilon_a = 0.75 - 2.5\ 10^{-5} h_s \quad (12)$$

The cloud contribution is written as:

$$L_c = \epsilon_{cl} \sigma n f T_c^4 \quad (13)$$

$$f = -0.6732 + 6.24\ 10^{-3} T_c - 0.914\ 10^{-5} T_c^2 \quad (14)$$

A constant lapse rate (0.7°/100 m) and a constant cloud base height (3500 m) are used to relate the cloud base temperature to the air temperature:

$$T_c = T_a + \Gamma h_{cl} \quad (15)$$

The outgoing longwave radiation is based on the principal that the ice/snow surface radiates as a black body in the infra-red:

$$L_o = \sigma T_s^4 \quad (16)$$

Because no englacial temperature profile is calculated, a parameterization for the surface temperature has to be adopted:

$$T_s = \bar{T}_a - A_t \cos\left(\frac{2\pi(day - 3)}{365}\right) - C_t \cos\left(\frac{2\pi t}{24}\right) \quad T_s \leq 0 \quad (17)$$

This relation is based on the idea that the surface temperature increases or decreases stronger during the day, as long as no melting occurs. The surface temperature is of course limited by the melting point of ice. No data are available to justify the simplified treatment of the surface temperature but we consider this parameterization to be accurate enough for the present level of detail in the model.

Turbulent heat flux

The turbulent heat flux is taken proportional to the difference between air temperature and surface temperature:

$$F_l = C(T_a - T_s) \quad (18)$$

$$C = 10 \text{ for } x = 0$$

$$C = 7.5 \text{ for } x = 20 \quad (19)$$

$$C = 2.5 \text{ for } x > 20$$

In this parameterization the exchange coefficient is a function of the distance to the ice margin. Measurements along a profile near Søndre Strømfjord show a decreasing turbulent heat flux towards the equilibrium line. The value of 10 W m^2 K^{-1} is in the range usually found in the literature. Note that, due to the definition of the surface temperature, (T_s in Eq. 16), the turbulent heat flux is zero, integrated over a day in winter time if $T_s \ll 0$. In summer, close to the ice margin, T_s approaches zero and the turbulent heat flux will add energy to the surface.

10. List of symbols

A_t	amplitude of the annual air temperature (°C)
B_t	amplitude of the daily air temperature (°C)
C_t	amplitude of the daily surface temperature (°C)
C	turbulent exchange coefficient (W m^{-2} K^{-1})
day	day number (starting January, 1)
f	fraction of black body radiation in atmospheric window
F_l	turbulent heat flux (W m^{-2})
h_{cl}	height cloud base (m.a.s.l.)
h_{inv}	inversion height (m.a.s.l.)
h_s	surface elevation (m.a.s.l.)
L_c	contribution to the terrestrial radiation from clouds (W m^{-2})
L_i	incoming terrestrial radiation (W m^{-2})
L_o	outgoing terrestrial radiation (W m^{-2})
n	cloud cover
Q	global radiation (W m^{-2})
S	shortwave radiation at the top of the atmosphere (W m^{-2})
t	local solar time (hr)
T_a	air temperature (°C)
T_c	temperature of cloud base (K)

T_s surface temperature (°C)
x distance from the ice margin (km)
Z zenith angle (degrees)
ϵ_a clear sky emittance
ϵ_{cl} cloud emittance
Γ temperature lapse rate (K m^{-1})
τ_a clear-sky transmissivity for solar radiation
τ_c cloud transmissivity for solar radiation
cl latitude (°N)
σ Stefan Boltzman constant (W m^{-2} K^{-4})

11. References

Ambach, W., 1963. Untersuchungen zum Energieumsatz in der Ablationszone des Grönlandischen Inlandeises. Medd. Grønl., 174 (4), 311 pp.

Ambach, W., 1979. Zur Nettoeisablation in einem Höhenprofil am Grönlandischen Inlandeis. Polarforschung, 49: 55–62.

Ambach, W. and Kuhn M., 1989. Altitudinal shift of the equilibrium line in Greenland calculated from heat balance characteristics. In: J. Oerlemans (Editor), Glacier Fluctuations and Climatic Change. Kluwer, Dordrecht, pp. 281–288.

Braithwaite, R.G. and Olesen, O.B., 1984. Ice ablation in West Greenland in relation to air temperature and global radiation. Z. Gletscherk Glazialgeol., 20: 155–168.

Braithwaite, R.G. and Olesen, O.B., 1989. Calculation of glacier ablation from air temperature, West Greenland. In: J. Oerlemans (Editor), Glacier Fluctuations and Climatic Change. Kluwer, Dordrecht, pp. 219–234.

Braithwaite, R.J. and Olesen, O.B., 1990. Increased ablation at the margin of the Greenland Ice Sheet under a greenhouse-effect climate. Ann. Glaciol., 14: 20–22.

Dibb, J.E., 1992. The accumulation of ^{210}Pb at Summit, Greenland since 1855. Tellus, 44B: 72–79.

Duynkerke, P.G. and Van den Broeke, M., 1994. Surface energy balance and atmospheric boundary layer structure near the boundary line between glacier and tundra during GIMEX 91. Global Planet. Change, 9: 17–28.

Greuell, J.W. and Oerlemans, J., 1989. Energy balance calculations on and near Hintereisferner (Austria) and an estimate of the effect of thegreenhouse warming on ablation. In: J. Oerlemans (Editor), Glacier Fluctuations and Climatic Change. Kluwer, Dordrecht, pp. 305–323.

Greuell, J.W., 1992. Numerical modelling of the energy balance and the englacial temperature at the ETH Camp, West Greenland. Züricher Geogr. Schr., 51.

Huybrechts, P., Letreguilly, A. and Reeh, N., 1991. The Greenland ice sheet and greenhouse warming. Palaeogeogr., Palaeoclimatol., Palaeoecol. (Global Planet. Change Sect.), 89: 399–412.

Kimball, B.A., Idso, S.B. and Aase, J.K., 1982. A model for thermal radiation from partly cloudy and overcast skies. Water Resour. Res., 18 (4): 931–936.

Konzelmann, T., Van de Wal, R.S.W., Greuell, J.W., Bintanja, R., Henneken, E. and Abe-Ouchi, A., 1994. Parameterization of short- and longwave incoming radiation for the Greenland Ice Sheet. Global Planet. Change, 9: 143–164.

Kuhn, M., 1979. On the computation of heat transfer coefficients from energy-balance gradients on a glacier. J. Glaciol., 22, 87: 263–271.

Kuhn, M., 1989. The response of the equilibrium line altitude to climate fluctuations: theory and observations. In: J. Oerlemans (Editor), Glacier Fluctuations and Climatic Change. Kluwer, Dordrecht, pp. 407–417.

Letréguilly, A., Huybrechts, P. and Reeh, N., 1991. Steady-state characteristics of the Greenland ice sheet under different climates. J. Glaciol., 37, 125: 149–157.

Oerlemans, J., 1991. The mass balance of the Greenland Ice Sheet: sensitivity to climate change as revealed by energy-balance modelling. Holocene, 1 (1): 40–49.

Oerlemans, J. and Vugts, H.F., 1993. A meteorological experiment in the melting zone of the Greenland ice sheet. Bull. Am. Meteorol. Soc., 74(3): 355–365.

Ohmura, A., 1987. New temperature distribution maps for Greenland. Z. Gletscherkd. Glazialgeol., 23 (1): 1–45.

Ohmura, A. and Reeh N., 1991. New precipitation and accumulation maps for Greenland. J. Glaciol., 37, 125: 140–148.

Putnins, P., 1970. The climate of Greenland. In: S. Orvig (Editor), World Survey of Climatology. 17. The Climate of the Polar Regions. Elsevier, Amsterdam, pp. 3–128.

Reeh, N., 1989. Dynamic and climatic history of the Greenland Ice Sheet. In: R.J. Fulton (Editor), Quaternary Geology of Canada and Greenland. Geol. Surv. Can., (1): 793–822.

Reeh, N., 1991. Parameterization of melt rate and surface temperature on the Greenland Ice Sheet. Polarforschung, 59 (3): 113–128.

Sauberer, F., 1955. Zur Abschätzung der Globalstrahlung in verschiedenen Höhenstufen der Ostalpen. Wetter und Leben, 7: 22–29.

Van den Broeke, M., Duynkerke, P.G. and J. Oerlemans, 1994. The observed katabatic flow at the edge of the Greenland Ice Sheet during GIMEX 91. Global Planet. Change, 9: 3–15.

Wal, v.d. R.S.W. and Russell, A.J., 1994. Energy balance calculations and meltwater runoff near Søndre Strømfjord, West Greenland. Global Planet. Change, 9: 00–00.

Walraven, R., 1978. Calculating the position of the sun. Solar Energy, 20: 393–397.

Warrick, R. and Oerlemans, J., 1990. Sea level rise. In: J.T. Houghton, G.J. Jenkins and J.J. Ephraums (Editors), Climatic Change, The IPCC Scientific Assessment. Cambridge Univ. Press, pp. 261–281.

Weidick, A., 1984. Studies of glacier behaviour and glacier mass balance in Greenland a review. Geogr. Ann., 66A (3): 183–195.